RECENT DEVELOPMENTS IN NUMERICAL MODELING OF COMPOSITE SOIL SYSTEMS WITH GEOGRID INCLUSIONS

Mohamed Meguid
Associate Professor &
Associate Dean,
Faculty of Engineering,
McGill University,
Montreal, Quebec,
H3A 0C3 Canada

Dr. Meguid is a Civil Engineer specializing in geotechnical engineering, engineering mechanics and non-linear soil-structure interaction. Recent research interests include the analysis and design of tunnels, buried pipes and culverts; and the development of innovative numerical methods to investigate the micromechanical behavior of granular soils in contact with surface and subsurface structures.

ABSTRACT

The advancement of geosynthetic technology over the past few decades has allowed for the successful use of reinforcement materials in constructing different types of earth-retaining structures. To avoid instability and other serviceability problems, a better understanding of the interaction mechanism between the reinforcement layer and the surrounding ground is needed. This keynote lecture reviews selected geomechanical aspects of HDPE geogrid material used to improve the performance of geotechnical structures. The first part of the lecture discusses the advantages and limitations of continuum mechanics in capturing the complicated nature of the material and its interaction with the surrounding ground. A three-dimensional nonlinear finite element analysis is conducted to simulate the interaction between a geogrid sheet and the backfill material. The geogrid geometry is explicitly modeled in this study to capture the different sources of pullout resistance in the composite system. An efficient finite-discrete element framework that allows for combining the particulate nature of the backfill material and the continuous nature of the geogrid is introduced and used to study the behavior of HDPE biaxial geogrid under pullout loading condition. In this framework, the geogrid is modelled using finite elements whereas the surrounding soil is simulated using discrete particles. The interaction between the two domains is ensured using interface elements. The interlocking mechanism and the stresses and displacements developing in the geogrid are discussed. Finally, recommendations for future modeling and analysis of similar composite soil systems are made.

Keywords: Soil reinforcement, HDPE geogrid, finite element, discrete element, multi-scale modelling, soil-structure interaction, buried structures.

INTRODUCTION

The use of extruded high density polyethylene (HDPE) inclusions as reinforcement material has proven to be economically attractive in various civil engineering applications including integral bridge abutments, mechanically stabilized earth retaining walls, and reinforced soil slopes. Geogrid is the generation of polymeric geosynthetics that is designed specifically for soil reinforcement due to their high tensile strength and the 3D open structure that creates interlocking effects with the surrounding soil. Stresses in the reinforcing elements are transferred to the surrounding soil through one of the following interaction (bonding) mechanisms: i) friction, ii) passive soil resistance, or iii) a combination of both. To maintain equilibrium, the induced bond must resist the maximum tensile load carried by the reinforcing element (pull-out resistance).

Figure 1 shows an example of a reinforced earth wall showing the different failure mechanisms that would develop due to failure of the reinforced system. One of the dominant failure modes (D) is pullout condition which is best represented using a pullout laboratory experiment.

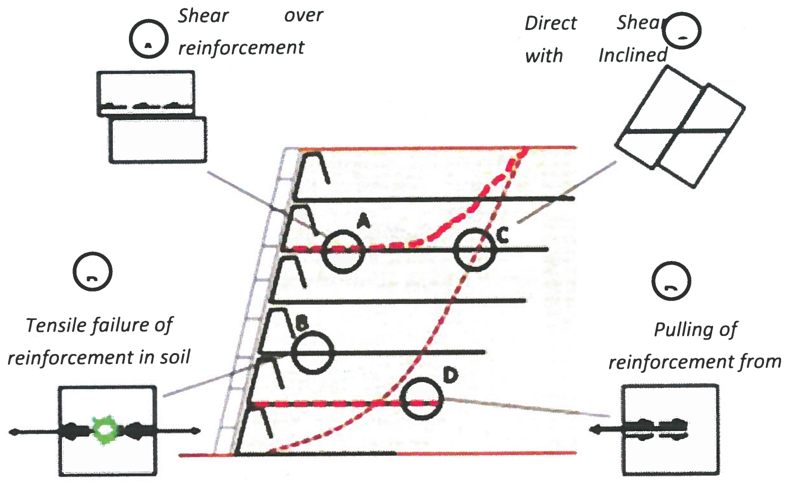

Figure 1. Tests required for different failure modes in a reinforced earth wall [1]

Jewell et al. [2] classified the different mechanisms in which reinforcement interacts with soils into three main mechanisms: a) skin friction along the reinforcement; b) soil-soil friction; c) passive (bearing) resistance on the transverse members of the reinforcement. Both theoretical and experimental studies have been used in the past few decades to investigate the response of reinforced soil systems under pullout loading condition [e.g. 3, 4, 5, 6, 7, 8, 9]. While it is possible to track the load-displacement response of a geogrid sheet in pullout experiments, the behavior of the backfill soil as it interacts with the geogrid material is hard to evaluate experimentally. Numerical methods are, therefore, considered more suitable for that purpose. Finite element (FE) is widely used as a numerical tool to model pullout procedure [10, 11]. The geogrid geometry is often simplified either as a truss structure (in 2D analysis) or a continuous sheet (in 3D analysis). Using these simplified approaches makes it difficult to separate the contributions of the frictional and bearing resistances with respect to the overall pullout capacity of a reinforced system. In addition, it would be challenging to determine the stress and strain distributions in the geogrid members as well as in the surrounding soil material. Hussein and Meguid [12, 13] modelled geogrid pullout test using 3D FE analysis capturing the detailed geometry of the embedded geogrid material. A brief summary of their modeling work is provided in the next section.

As an alternative to the continuum approach, the discrete element (DE) method has been used by several researchers to model soil-geogrid interaction. McDowell et al. [14] and Chen et al. [15] used DE to model both the geogrid and the backfill soil. In this approach, the geogrid is simulated using a set of spherical particles bonded together to form the geogrid shape. The interaction between the geogrid and the surrounding soil is obtained through the contact between discrete particles. Although microscopic parameters of the bonded geogrid particles are determined using index tests, the complex geogrid deformation may not be accurately captured due to the inflexibility of the used particles. Moreover, since a set of bonded particles are used to capture the continuous nature of the geogrid, the strains and stresses within the geogrid may not be accurately obtained.

To take advantage of both the FE and DE methods, the reinforcement layer can be modeled using FE whereas the backfill soil can be modeled using the DE method. The coupling of the two methods can efficiently model the behavior of the geogrid as well as the backfill soil material. This approach has been used to solve certain problems such as: geosynthetic reinforced earth structures [16], pile installation [17] and earth pressure on tunnel linings [18]. In this paper, a coupled finite-discrete element (FE-DE) framework is used to investigate the soil-geogrid interaction under pullout loading condition. The results of the numerical simulation including the detailed response of the geogrid and the surrounding soil are presented and compared with experimental data. Although emphasis is placed in this study on the frictional and bearing components of the pullout resistance, displacements, stresses, and strain fields in the vicinity of the geogrid layer are also highlighted. This numerical framework aims at helping researchers gain new insights into soil-structure interaction problems at the microscopic scale level.

MODELING PULLOUT TEST USING FINITE ELEMENT ANALYSIS

Numerical methods have been used by researchers to interpret laboratory data and develop a better understanding of soil geosynthetic interaction [19, 20, 21, 22]. It has been shown that the stress-strain behaviour of geosynthetic materials is complex and the constitutive model must contain a number of components to describe this behaviour. Therefore, successful numerical simulation of reinforced earth structures depends on selecting proper constitutive models for the soil, geosynthetic and soil-geosynthetic interface. A 2D model was developed by Yogarajah and Yeo [23] where the geosynthetic sheet was simulated using bar elements. Joint elements were used to model the interface between the geosynthetic layer and the soil. Shuwang et al. [24] proposed a 2D FE model for the soil-geogrid interaction subject to pull-out loading. The geogrid was treated as a nonlinear elastic plate with openings under plane stress condition and the interaction between the soil and geogrid was modeled using non-linear springs. Perkins and Edens [25] conducted FE analysis of a pullout test employing the constitutive model suggested by Perkins [26] for the geogrid layer and the bounding surface plasticity model for the soil. The geogrid was modeled using 4-noded membrane elements. Shear interaction between the geogrid and the aggregate was established using two contact surface pairs employing Coulomb frictional model. Results showed that the geosynthetic creep properties have a small effect on the geogrid response. The results did, however, show that plasticity had a more significant effect on the load-displacement relationship as the geosynthetic approaches failure. Siriwardane et al. [27] conducted 3D FE analysis to investigate the effect of the interface properties on the pull-out capacity where the geogrid was treated as linear elastic material using membrane elements.

Although the above studies explained several interesting features of the geogrid-soil interaction under pullout loading condition, they were mostly based on simplifying assumptions related to either the details of the geogrid geometry or the constitutive model of the geogrid material.

Unconfined Geogrid under Tensile Loading

To illustrate the importance of properly choosing a suitable geometric and material model in simulating embedded HDPE geogrid sheet under axial force, an experimental pull-out test performed on a uniaxial geogrid [28] is numerically modeled using FEA.

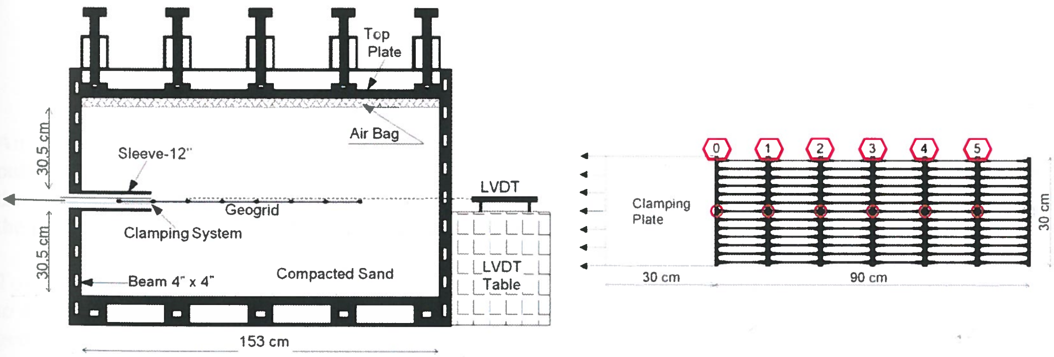

Figure 2. A cross section of the pull-out box and the instrumented uniaxial geogrid [28]

The inside dimensions of the box are 153 cm long, 61 cm high, and 90 cm wide. The width of the box was chosen to keep a standard geogrid sample, of 30 cm wide, at a distance of 30 cm from each side of the box. The front wall contains a slot (5 cm in height) to allow for the clamping plates to be pulled out of the box. An air bag 5 cm in thickness was used to apply vertical pressure over the soil. Pull-out displacement controlled tests with a rate of 6 mm/min were conducted using a confining pressure of 48 kN/m^2. The sand used in these experiments was uniform blasting sand. Standard specimen of 30 cm width x 90 cm length, which comprises 13 longitudinal elements and 7 transverse elements, was tested as shown in Figure (2). The pull-out load was applied through a non-deformable clamp attached to the front end of the geogrid specimen. The properties of the soil and geogrid are summarized in Table (1).

Sand	γty (kN/m^3)	E (MN/m^2)	ν	ϕ°	ψ°	c (kN/m^2)
	16.80	50	0.3	37	7	5
Geogrid						Yield stress (MN/m^2)
	85 x 10^{-5}	472	0.3	-	-	56
Interface Parameters		μ				E_{slip} tolerance
		0.50				0.005

Table 1. Input parameters used in the finite element analysis

A non-linear elastic-plastic constitutive model, that separates the elastic and plastic strains, was developed to simulate the true behaviour of the polymeric geogrid material. The properties of the generated model are determined by matching the experimental load-displacement curve obtained from index tests performed under a given displacement rate (3 mm/min). The developed model allows for the non-linear elastic response of the geogrid to be captured such that it agrees with the experimental data. The behaviour of the soil-geogrid interface was simulated using the Coulomb friction model with two material parameters- a friction coefficient (μ), and a tolerance parameter (E_{slip}).

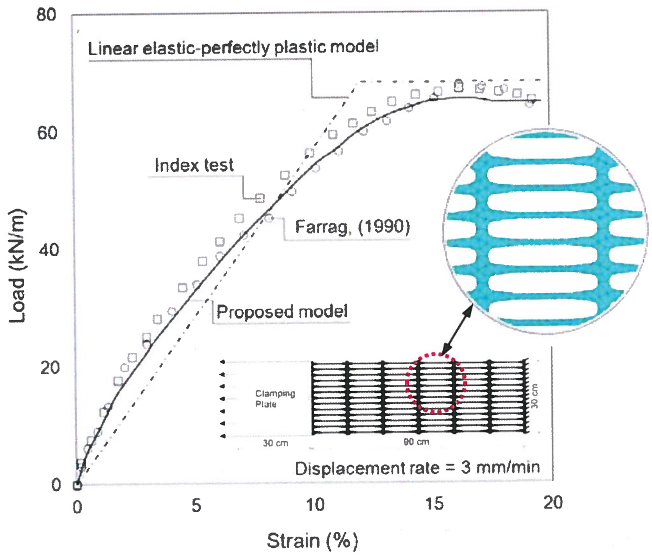

Figure 3. In-air (unconfined) response of geogrid under tensile loading

To measure the efficiency of the developed constitutive model, the predicted response of the geogrid was compared with experimental data as well as index test results provided by the manufacturer as shown in Figure 3. The response calculated using the conventional linear elastic-perfectly plastic model has also been added for comparison purposes. It can be seen that the linear elastic-perfectly plastic model was not able to capture the nonlinear behavior of the geogrid particularly at small strains. The predicted response using the developed nonlinear model provided a better agreement with the measured results in both the elastic as well as the plastic regions. The model is capable of capturing the material nonlinearity in addition to the ultimate strength of the tested geogrid sample.

Embedded Geogrid Subjected to Pullout Loading

To examine the role of geogrid geometry in resisting the pull out forces, a simple 2D finite-element model was first developed using ABAQUS and used to calculate the load-displacement behavior of the embedded geogrid sheet. The geogrid is modelled using line elements with equivalent properties. The configuration of the experiment was used to define the dimensions and boundary conditions of the numerical model including the box, rigid sleeve, geogrid, etc.

The load-displacement behaviour of the embedded geogrid layer during the pull-out test is presented in Figure 4. In general, a softer geogrid response was noticed as compared to the in-air test with a maximum load of about 30 kN/m at failure. It can be seen that, despite the fact that the correct material model for the geogrid has been used in the analysis, the calculated response using 2D truss elements did not capture the geogrid displacement or the ultimate pull-out strength of the geogrid material.

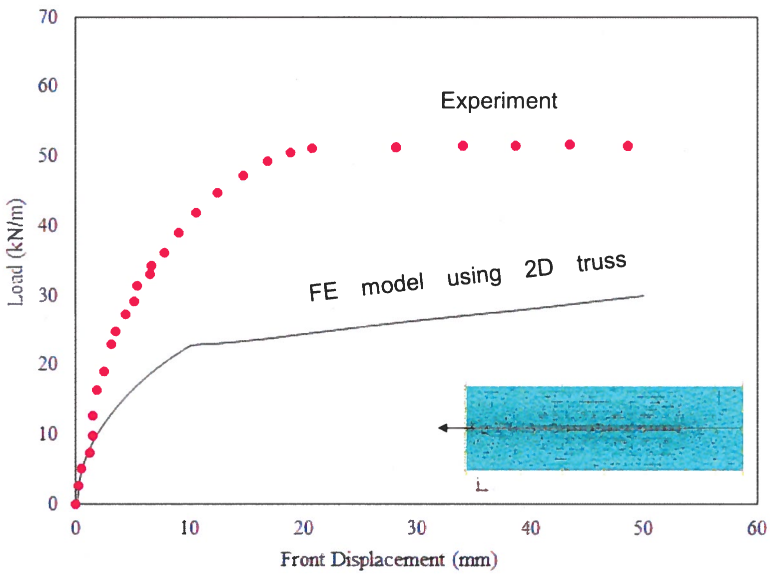

Figure 4. Pullout load-displacement relationship using 2D truss elements for the geogrid

An alternative approach is to use a 3D model with continuous sheet representing the geogrid material. The pullout load is plotted against frontal displacement and the results are shown in Figure 5. It can be seen that the model reasonably predicted the stiffness of the system at small strain. In addition, an improvement in the ultimate strength was found with a maximum pullout load of 40 kN/m.

To overcome the above limitations, a full 3D finite element model was developed using ABAQUS software to simulate the pull-out experiment. The model was divided into three main parts; the top soil (above the geogrid), the bottom soil (below the geogrid) and the geogrid layer. The analysis was performed using six-nodded solid elements for the soil and 3-noded triangular membrane elements for the geogrid. In order to simulate the actual configuration of the experiment, the dimensions and properties of different components (box, sleeve, geogrid, etc.) were chosen such that they represent those used in the actual test.

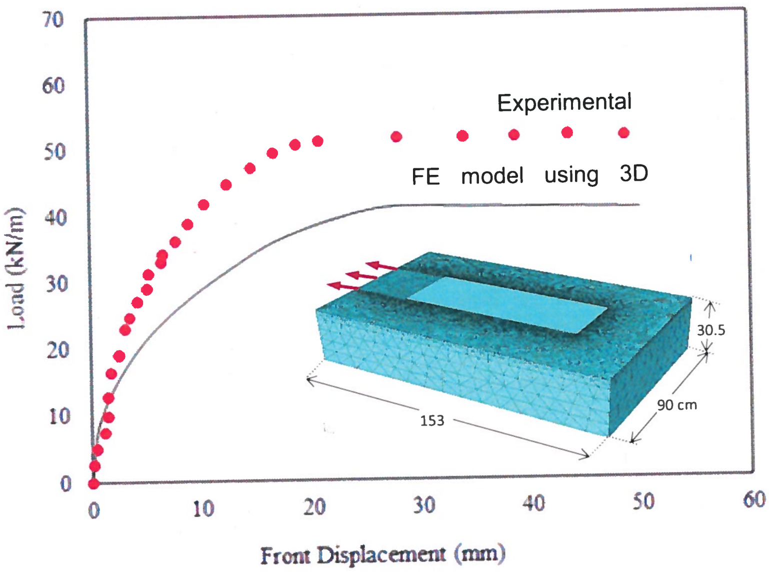

Figure 5. Pullout load-displacement relationship using continuous sheet the geogrid

It should be noted that the details of the grid apertures were taken into account in this study to capture the discontinuous nature of geogrid sheet. The Mohr-Coulomb model as implemented in ABAQUS was used for the sand material adopting a non-associated flow rule. Shear interaction between the geogrid and the soil was established by creating two contact surface pairs above and below the geogrid. Coulomb friction model was used to simulate this interaction with two material parameters- friction coefficient, and tolerance parameter.

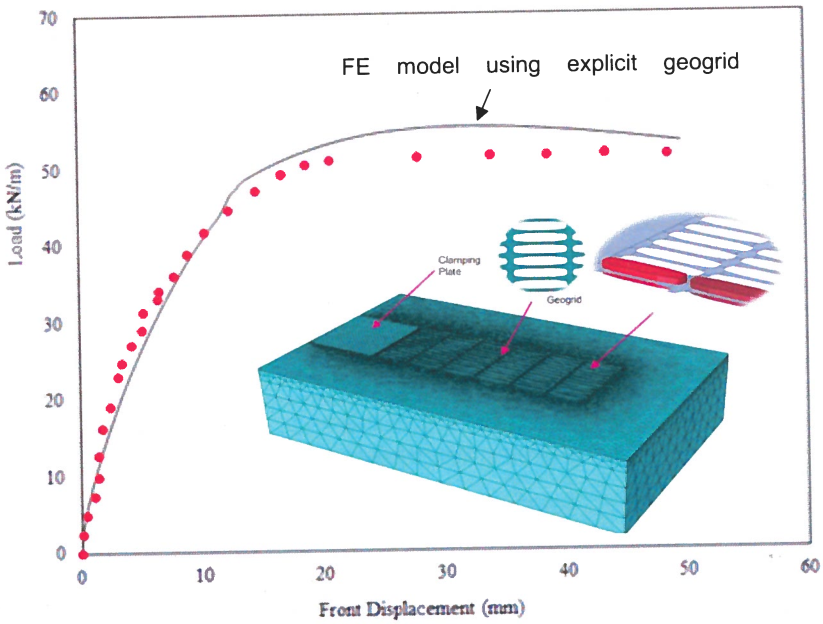

Figure 6. Pullout load-displacement relationship using true geogrid geometry

ture the
as used
and the
friction
lerance

The relationship between the pull-out force and the frontal displacement for the embedded geogrid obtained from both the experimental and numerical models is shown in Figure 6. The model configuration coupled with the developed geogrid material model allowed for the soil-geogrid interaction to be captured for the entire loading range up to 50 kN/m.

The geogrid pullout capacity comprises two components- frictional resistance ($P_{s/r}$) and passive bearing (P_{pb}). Each of these components contributes to the total pull-out resistance with various weights. Contribution of each component to the total pull-out resistance is shown in Figure 7.

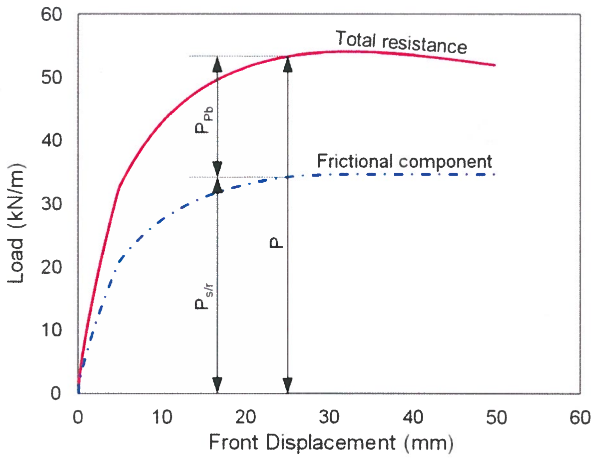

Figure 7. Components of the pullout resistance based on 3D FE analysis

The total resistance was obtained by relating the pullout load to the front displacement, whereas, the frictional resistance component was calculated by eliminating the contact force on the transverse members such that no bearing resistance exists. From Figure 7, it can be seen that the difference between the total pull-out force and the frictional resistance is about 36% which reflects the contribution of the bearing resistance compared to the total pull-out resistance of the geogrid.

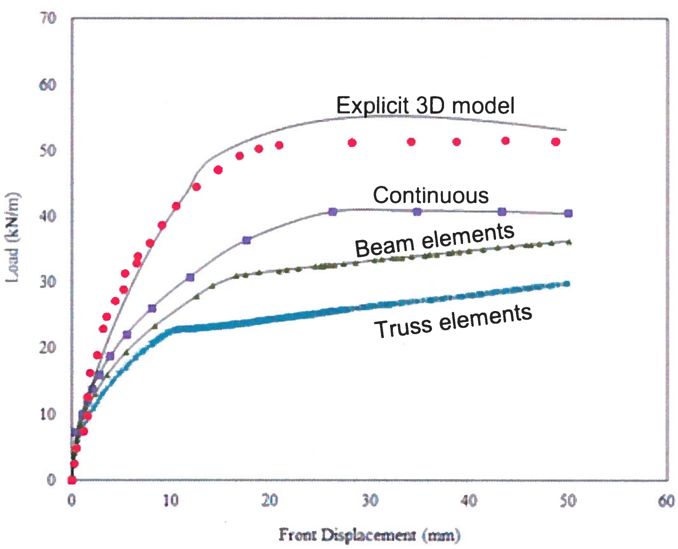

Figure 8. Comparison between the different FE models in simulating pullout response

A comparison between the calculated pullout response using different finite element models is shown in Figure 8 along with the measured experimental data. It can be seen that the 2D analysis and 3D sheet elements did not predict the correct pullout load. In addition the 3D model using grid geometry was found to predict the stiffness of the composite system as well as the ultimate pullout load.

Although the finite element analysis conducted using explicit 3D geogrid geometry has reasonable simulated the pullout response and predicted a load-displacement relationship that is consistent with the experimental data, the analysis required extensive computing resources and was found to be generally expensive. This is attributed to the high nonlinearity of the system. The nonlinearly did not only result from the material models adopted but also from the contact properties and the relative movements at the interface. In addition, the response was only reliable at the front face of the box as finding stresses and displacements within the composite system is challenging.

MODELING GEOGRID INCLUSIONS USING FINITE-DISCRETE ELEMENT ANALYSIS

A framework that takes advantage of both FE and DE has been developed by Dang and Meguid [18] and further used to model soil-geogrid interaction [29]. In this section, an experimental pullout test performed on a geogrid type SS-1 [30] is adopted and numerically modeled using the proposed coupled FE-DE model. The soil container was reported to be 0.68 m in length, 0.3 m in width and 0.625 m in height. The front wall composed of six acrylic plates each of 0.3 m wide and 0.1 m height to reduce the soil-wall friction. The soil used in the experiment was Silica Sand No. 5 with D_{50} = 0.34 mm and a peak friction angle of 29.9° as obtained from laboratory triaxial tests. A geogrid specimen (Tensar SS-1 with polypropylene material and stiffness 285.6 kN/m at a strain of 3%) of 500 mm in length and 300 mm in width was used throughout the experiments. The sand was placed in layers using the raining technique and the pullout load was applied through a clamp attached to the front end of the geogrid sheet.

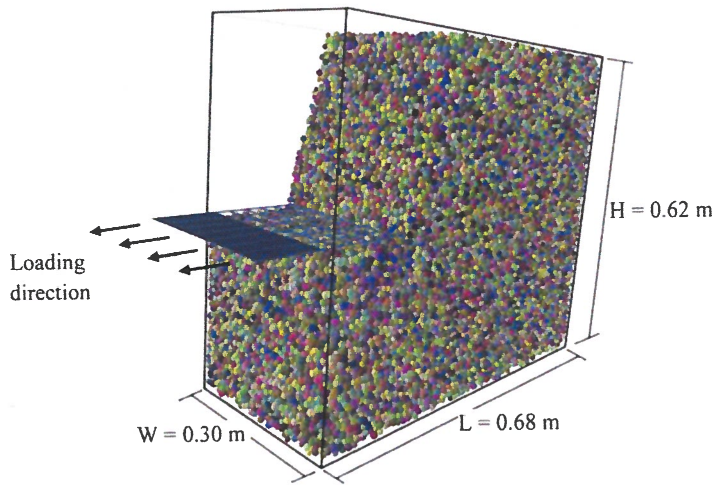

Figure 9. FE-DE model for the pullout test

Vertical stresses 49 kPa and 93 kPa were applied above and below the box using air bags to prevent vertical movement of the geogrid during the test. The geogrid was pulled out at a constant rate of 1.0 mm/min and both the load and lateral movement were measured using load cells and displacement gauges, respectively. The numerical model has been developed such that it follows the geometry and test procedure used in the actual experiment. The geogrid is modeled using FE while the soil is modeled using DE, as discussed in Section 2. Interface elements are used to simulate the interaction between the two domains. All components are generated inside YADE using two corresponding FE and DE packages. The biaxial SS-1 geogrid, which comprises 8 longitudinal elements and 19 transverse elements, is modeled using 8-noded brick elements with 8 integration points (Figure 9). A non-deformable clamp is introduced at one end of the geogrid. The initial distance between the front wall and the 1st transverse member is 30 mm to ensure that all transverse members remain within the soil domain during the test (the maximum applied pullout displacement is 25 mm). A linear elastic material model is used for the geogrid sheet and its properties are determined by matching the experimental load-displacement curve obtained from the conducted index tests at a medium strain of 2% (as shown in Table 1). It is noted that the local increase in joint thickness is not considered in the geogrid model in order to simplify the analysis. The full geometry of the geogrid comprising over 1300 finite elements and 20,000 interface elements is shown in Figure 9.

The model is validated by comparing the calculated and measured displacements along the geogrid as shown in Figure 10. It can be seen that geogrid displacements decrease with distance from the face. For all examined frontal displacements the geogrid movement (Ux) occurs within a limited region from the front side to about the middle of the geogrid. Very small displacements were calculated outside this region. The results also confirms the agreement between the measured and calculated displacement using the proposed framework.

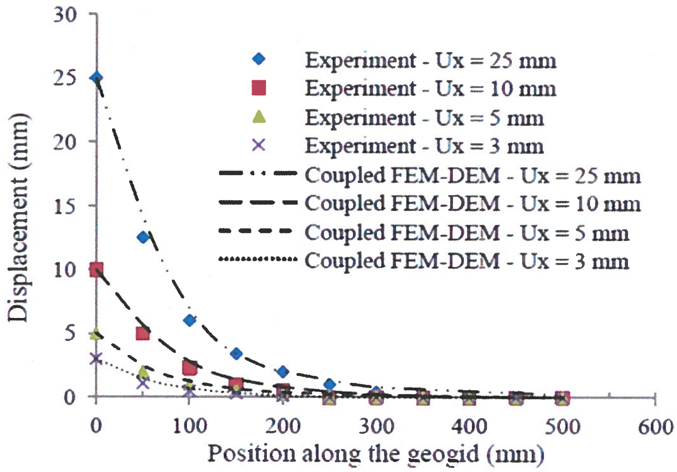

Figure 10. Horizontal displacements along the geogrid (σ_v = 49 kPa).

Geogrid Response to Pullout Loading

The deformed shape of the geogrid for a frontal displacement (U_x) of 10 mm and a vertical pressure (σ_v) of 49 kPa is shown in Fig. 11a. The largest deformation of the geogrid is found to occur in the vicinity of the applied load and rapidly decreases with distance toward the rear side of the box. The longitudinal elements of the geogrid experienced deformation in its axial direction with the largest elongation occurring near the loading side. It is also noted that part of the geogrid that is connected to the loading clamp has to be in air during the test which results in softer behavior and larger elongation in that region. Transverse members, on the other hand, showed a dominant bending deformation particularly near the loaded side. This bending behavior originates from the frictional forces acting at the upper and lower geogrid surfaces as well as the bearing forces acting as the geogrid pushes against the soil.

The stress distribution within the geogrid is shown in Fig. 11b. In consistency with the displacement pattern, the stresses S_{xx} were highest near the front side and rapidly decreased to a negligible value at a distance of about 50% of the geogrid length. It can be also realized that stresses in the longitudinal members are much larger compared to the transverse ones.

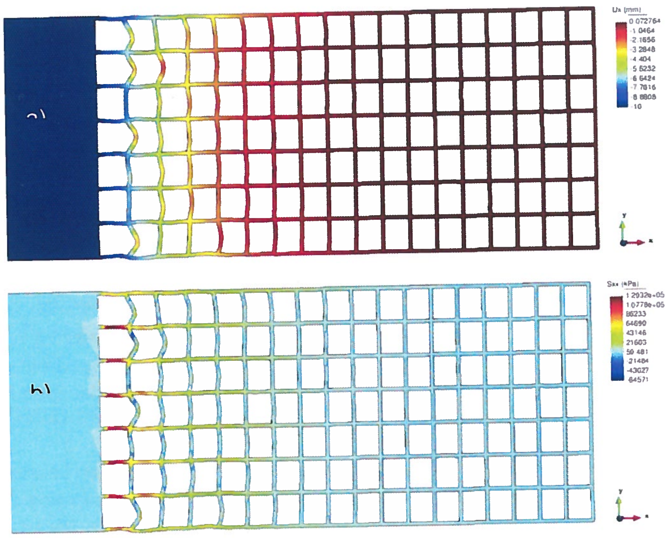

Figure 11. a) Geogrid deformation; and b) Geogrid stresses at U_x = 10 mm and σ_v = 49 kPa

The tensile force distributions in the longitudinal members for different frontal displacements are illustrated in Fig. 12. At a given location along the geogrid, the average tensile force (P_{xx}) in all longitudinal members was found to increase with the increase in frontal displacements. For the investigated range of frontal displacements, the force P_{xx} was large near the front side and rapidly decreased toward the middle of the geogrid. Beyond the middle zone, P_{xx} became negligible due to the insignificant displacement experienced by the rest of the geogrid.

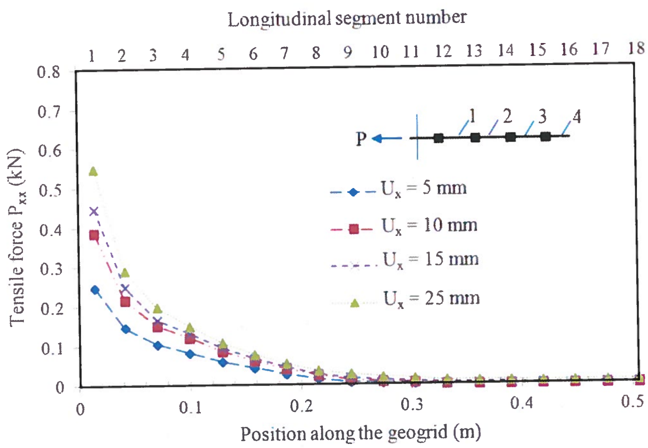

Figure 12. Average tensile force P_{xx} in the longitudinal members (σ_v = 49 kPa).

Fig. 13 shows the displacement field across the soil domain at a frontal displacement of 10 mm. It can be seen that most of the soil movement developed near the front face of the box leading to soil densification in that area. Soil movement gradually decreased and became negligible around the middle of the geogrid. Particles in the vicinity of the geogrid tend to move horizontally toward the front face. This movement gradually changes to the vertical direction near the front face where particles displace away from the geogrid layer. These observations agree well with the results of the X-ray radiographs reported by Alagiyawanna et al. [30]. Similar soil movement pattern in pullout tests has also been reported by Jewell

[31] and Dyer [32]. The contact force networks within the soil domain for both a) initial condition; and b) for frontal displacement of 10 mm are shown in Fig. 14. Each contact force is illustrated by a line connecting the centers of two contacting elements while the width of the line is proportional to the magnitude of the normal contact force. For the initial condition, most of the contact forces are oriented vertically in response to the applied pressure above and below the soil sample. As the geogrid is pulled out, soil particles started to move resulting in an increase in contact forces in the horizontal direction while the magnitudes of the contact forces in the vertical direction are maintained. This newly introduced horizontal component resulted in the development of diagonal contact forces as shown in Fig. 14b. Contact forces that originate from the geogrid have larger values as they transmit forces from the geogrid to the surrounding soil. Large contact forces are observed in the vicinity of the front face in consistency with the soil densification near the vertical boundary. The contact force distribution is in agreement with the distributions observed by Dyer [32] using the photo-elasticity approach.

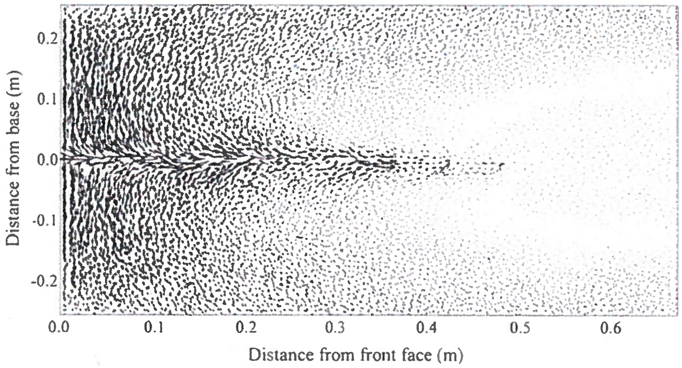

Figure 13. Displacement field of the soil domain at U_x = 10 mm and σ_v = 49 kPa.

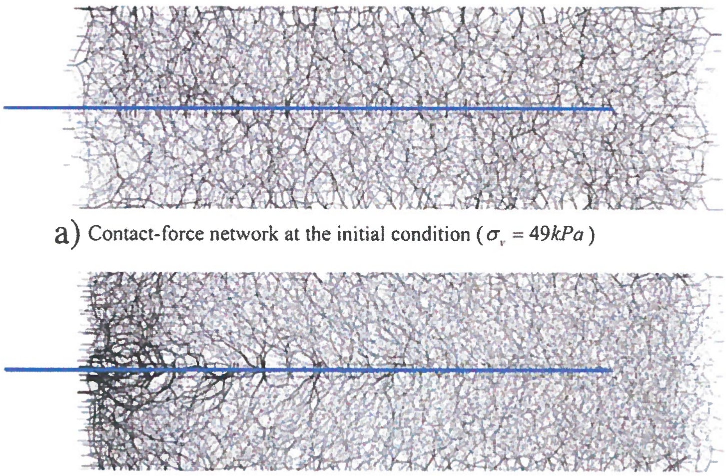

a) Contact-force network at the initial condition ($\sigma_v = 49kPa$)

b) Contact-force network at U_x = 10 mm ($\sigma_v = 49kPa$)

Figure 14. Contact force networks within the soil around the geogrid

The strain field within the soil domain is achieved using a tessellation approach [33, 34] and the results are shown in Fig. 15. It can be seen that strains developed mostly in the vicinity of the geogrid with the largest strain values near the front face of the pullout box.

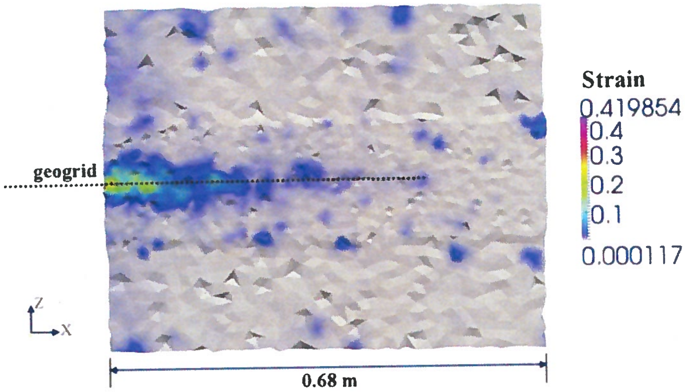

Figure 15. Strain field within the soil domain at U_x = 10 mm and σ_v = 49 kPa.

The stress distributions around the geogrid are shown in Fig. 16. For all examined frontal displacements, a increase in both the vertical and horizontal stresses is calculated with maximum increase in the clos vicinity of the front face of the box. This increase may be attributed to the use of horizontal plates to contrc the vertical pressure. Beyond approximately half the geogrid length measured from the front face, stresse remain close to their initial values. It can be seen that for the pullout test described in this study, the exter of the affected area under pullout load is generally limited to about 50% of the geogrid length.

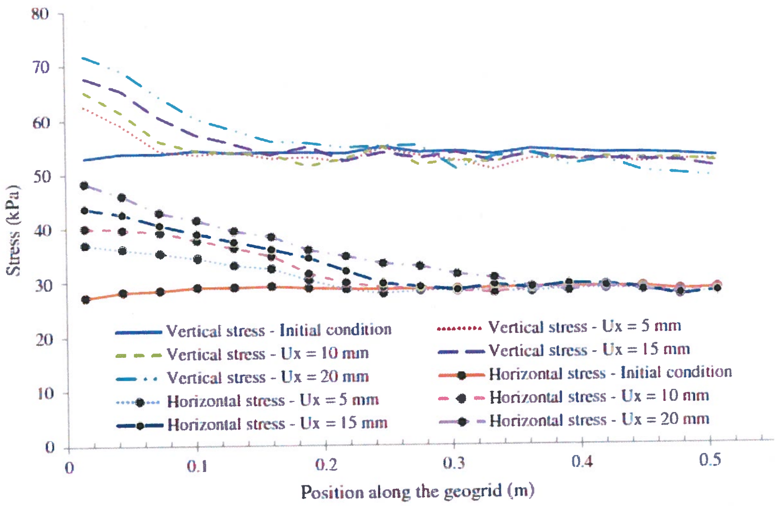

Figure 16. Distribution of the vertical and horizontal stresses in the soil (pressure σ_v = 49 kPa)

CONCLUSIONS

Finite element analysis can be used to analyze problems involving soil-geogrid interaction, however, appropriate constitutive model for the geogrid that captures the material nonlinearity is required. A framework for coupling finite and discrete element methods was developed. Interface elements were introduced to ensure the transmission of forces between the DE and FE domains. Using the developed framework, a three-dimensional numerical study was performed to investigate the behavior of a biaxial geogrid embedded in granular material under pullout loading condition. The geogrid was modeled using finite elements whereas the backfill material was modeled using discrete elements. The results of the analysis were compared with experimental data. The displacements and stresses developing in the geogrid were analyzed and the micromechanical behavior of the particles forming the soil domain was investigated.

Most of the geogrid stresses and displacements occurred near the front side of the box with rapid decrease with distance and reached very small values around the middle of the geogrid. For the investigated geogrid and soil conditions, the contribution of the frictional resistance to the total pullout resistance was found to be larger than the bearing resistance. The contribution of the bearing resistance to the overall capacity increased as the geogrid displacement increased. The soil movement and the contact force distribution within the soil domain agreed with experimental observations. An increase in soil stresses and strains was observed near the front face.

REFERENCES

1. Palmeira, EM. Soil-Geosynthetic Interaction: Modelling and Analysis, Geotextiles and Geomembranes, 2009; 27(5): 386-390.
2. Jewell, RA, Milligan, GWE, Sarsby, RW, and Dubois, D. Interaction between soil and geogrids, Proceedings of the Conference on Polymer Grid Reinforcement, Thomas Telford Publishing, London, 1984; 18-30.
3. Palmeira, EM, and Milligan, GWE. Scale and other factors affecting the results of pull-out tests of grids buried in sand, Geotechnique, 1989; 39(3): 511-524
4. Farrag, K, Acar, YB, and Juran, I. Pull-out resistance of geogrid reinforcements, Geotextiles and Geomembranes, 1993; 12: 133-159.
5. Bergado, DT, Chai, JC, Abiera, HO, Alfaro, MC, and Balasubramaniam, AS. Interaction between cohesive-frictional soil and various grid reinforcements, Geotextiles and Geomembranes, 1993; 12: 327-349.
6. Bakeer, RM, Sayed, MS, Cates, P, and Subramanian, R. Pullout and shear tests on geogrid reinforced lightweight aggregate, Geotextiles and Geomembranes, 1998; 16: 119-133.
7. Sugimoto, M, Alagiyawanna, AMN and Kadoguchi, K. Influence of rigid and flexible face on geogrid pullout tests, Geotextiles and Geomembranes, 2001; 19: 257-277.
8. Moraci, N, and Recalcati, P. Factors affecting the pullout behaviour of extruded geogrids embedded in a compacted granular soil, Geotextiles and Geomembranes, 2006; 24: 220-242.
9. Sieira ACCF, Gerscovich DMS, Sayao ASFJ. Displacement and load transfer mechanisms of geogrids under pullout condition. Geotextiles and Geomembranes, 2009; 27: 241-253.
10. Sugimoto, M, and Alagiyawanna ANM. Pullout behavior of Geogrid by Test and Numerical Analysis. Journal of Geotechnical and Geoenvironmental Engineering, 2003; 129(4): 361-371.
11. Khedkar, MS, and Mandal, JN. Pullout behaviour of cellular reinforcements. Geotextiles and Geomembranes, 2009; 27: 262-271.
12. Hussein, M, and Meguid, MA. On the three-dimensional modeling of soil-geogrid interaction. 62nd Canadian Geotechnical Conference, Halifax, September 2009, CD, 6 pages.
13. Hussein, M, and Meguid, MA. Three-Dimensional Finite Element Analysis of Soil-Geogrid Interaction under Pull-out Loading Condition. GeoMontreal, September 2013, Montreal, Quebec, 7 pages.
14. McDowell, GR, Harireche, O, Konietzky, H, Brown, SF, Thom, NH, Discrete element modelling of geogrid-reinforced aggregates, Proceedings of the ICE-Geotechnical Engineering, 2006; 159(1): 35-48.
15. Chen, C, McDowell, GR, Thom, NH. Discrete element modelling of cyclic loads of geogrid-reinforced ballast under confined and unconfined conditions. Geotextiles and Geomembranes, 2012; 35: 76-86.
16. Villard, P, Chevalier, B, Hello, BL, Combe, G, Coupling between finite and discrete element methods

for the modelling of earth structures reinforced by geosynthetic. Computers and Geotechnics, 2009; 36(5): 709-717.

17. Elmekati, A, Shamy, UE. A practical co-simulation approach for multiscale analysis of geotechnical systems. Computers and Geotechnics, 2010; 37(4): 494-503.
18. Dang, HK, Meguid, MA. An efficient finite-discrete element method for quasi-static nonlinear soil-structure interaction problems. International Journal for Numerical and Analytical Methods in Geomechanics, 2013; 37(2): 130-149.
19. Yogarajah, I, and Yeo, KC. Finite element modeling of pull-out tests with load and strain measurements, Geotextiles and Geomembranes, 1994; 13: 43-54.
20. Shuwang, Y, Shouzhong, F, and Barr, B. Finite-element modelling of soil-geogrid interaction dealing with the pullout behaviour of geogrids, ACTA Mechanica Sinica (English Series), Chinese Journal of Mechanics, 1998; 14(4): 371-382.
21. Sugimoto M, and Alagiyawanna AM N. Pullout behavior of geogrid by test and numerical analysis, Journal of Geotechnical and Geoenvironmental Engineering, 2003; 129(4): 361-371.
22. Perkins, SW, and Edens, MQ. Finite element modeling of a geosynthetic pullout test, Geotechnical and Geological Engineering, 2003; 21: 357-375.
23. Yogarajah, I, and Yeo, KC. Finite element modeling of pull-out tests with load and strain measurements, Geotextiles and Geomembranes, 1994; 13: 43-54.
24. Shuwang, Y, Shouzhong, F, and Barr, B. Finite-element modelling of soil-geogrid interaction dealing with the pullout behaviour of geogrids, ACTA Mechanica Sinica (English Series), Chinese Journal of Mechanics, 1998; 14(4): 371-382.
25. Perkins, SW, and Edens, MQ. Finite element modeling of a geosynthetic pullout test, Geotechnical and Geological Engineering, 2003; 1: 357-375.
26. Perkins, SW. Constitutive modeling of geosynthetics, Geotextiles and Geomembranes, 2000; 18: 273-292.
27. Siriwardane, H, Gondle, R, Kutuk, B, and Ingram, R. Experimental investigation and numerical analysis of reinforced geologic media, The 12th Int. Conf. of International Association for Computer Methods and Advances in Geomechanics (IACMAG), Oct., 2008, Goa, India, 4369-4379.
28. Farrag, K, Acar, YB, and Juran, I. Pull-out resistance of geogrid reinforcements, Geotextiles and Geomembranes, 1993; 12: 133-159.
29. Tran, V, Meguid, MA, and Chouinard LE, A finite-discrete element framework for the 3D modeling of geogrid-soil interaction under pullout loading conditions. Geotextiles and Geomembranes, 2013; 37: 1-9.
30. Alagiyawanna, AMN, Sugimoto, M, Sato, S, Toyota, H. Influence of longitudinal and transverse members on geogrid pullout behaviour during deformation. Geotextiles and Geomembranes, 2001; 19(8), 483-507.
31. Jewell, R, Some Effects of Reinforcement on Soils. PhD. thesis, 1980, University of Cambridge, UK.
32. Dyer, MR. Observations of the Stress Distribution in Crushed Glass with Applications to Soil Reinforcement. D.Phil. thesis, 1985, University of Oxford, Oxford, UK.
33. Bagi, K. Analysis of microstructural strain tensors for granular assemblies. International Journal of Solids and Structures, 2006; 43(10), 3166-3184.
34. Smilauer, V, Catalano, E, Chareyre, B, Dorofeenko, S, Duriez, J, Gladky, A, Kozicki, J, Modenese, C, Scholtès, L, Sibille, L, Stránský, J, Thoeni, K. Yade Documentation. The Yade Project, 2010; http://yade-dem.org/doc/.